Investigation of momentum correction factor in the swash flow

Fangfang Zhu[1], Nicholas Dodd[2], Magnus Larson[3], and Jie Zhang[4]

[1] University of Nottingham Ningbo China, 199 Taikang East Road, Ningbo, 315100, China. Email: fangfang.zhu@nottingham.edu.cn

[2]Faculty of Engineering, University of Nottingham, Nottingham NG7 2RD, UK. Email: nicholas.dodd@nottingham.ac.uk

[3]Water Resources Engineering, Lund University, Box 118, 22100, Lund, Sweden. Email: magnus.larson@tvrl.lth.se

[4]School of Naval Architecture and Ocean Engineering, Jiangsu University of Science and Technology, Zhenjiang 212100, China. Email: jie.zhang@just.edu.cn

ABSTRACT

Swash flows are commonly modelled using the Nonlinear Shallow Water Equations (NSWEs). In the derivation of the NSWEs, directly from depth-averaging the Navier-Stokes equations, a so-called momentum correction factor, β, emerges. In this study we present a numerical model of the NSWEs that includes β, which is allowed to vary in space and time, and feedback onto the flow. We apply this model to a swash flow, by making use of the vertical flow structure calculated by use of the log-law boundary layer and free flow region. We thereby examine its influence on the swash flow predictions in the dam-break swash event by Kikkert et al. (2012). The numerical results show that the momentum correction factor has a significant impact on the shoreline motion, and flow adjacent to the shoreline, which results in an over-prediction of the shoreline with respect to the standard ($\beta = 1$, NSWE) approach. Given that consideration of β should yield a more complete description of the swash dynamics, the implication is that the log-law boundary layer model does not describe the flow structure in the swash tip region well. The implication of this is that to achieve

accurate modelling at the flow uprush tip, at which point the largest bed shear stresses are typically exerted, a different submodel is required in that vicinity. Equally, it suggests that classical NSWEs also cannot describe the flow at the tip well, and that accurate prediction is achieved despite this inherent deficiency.

INTRODUCTION

The swash zone is the region adjacent to the moving shoreline that is quasi-periodically wetted and dried, and in which the flow is shallow and rapidly changing. Swash flows can be well described by Nonlinear Shallow Water Equations (NSWEs), as shown by many studies (Brocchini and Dodd 2008; Briganti et al. 2016; Incelli et al. 2016). The NSWEs are derived from Navier-Stokes equations by integrating over the water column, and applying the condition that the depth of water is very small compared with the wavelength. The integration over the water column yields the dependent variables for the NSWEs: water depth, and depth-averaged velocity.

The swash flow is shallow, and the drag effect of the beach over which it flows becomes important as the bottom bed shear stress becomes significant compared to the inertial force. The bed shear stress in turbulent flows is commonly roughly approximated by a Chezy law and included in the NSWEs. Such numerical studies show that the maximum run-up is greatly reduced if bed shear stress is included (Zhu and Dodd 2013; Zhu and Dodd 2015). The fact that bed shear stress exists, in swash flows is, however, synonymous with the fact that the velocity is not in fact depth uniform. Moreover, Baldock (2018) analysed existing PIV velocity profile data, and concluded that the boundary layer is well or fully developed in the upper swash zone, which implies the flow velocity there is partly or fully nonuniform in depth.

Navier-Stokes models solved in 2D (propagation and vertical directions) (Puleo et al. 2007; Torres-Freyermuth et al. 2013; Pintado-Patiño et al. 2015) can more accurately describe the boundary layer and the swash flow, but is much more computationally expensive compared to models based on NSWEs. In order to retain the simplicity of NSWEs framework and accuracy of describing the bottom boundary layer, a number of studies coupled the NSWEs with a sub boundary layer model (Barnes and Baldock 2010; Briganti et al. 2011; Zhu et al. 2022), which can describe the flow in the boundary layer more comprehensively compared to the Chezy law. In particular, in Zhu et al. (2022), who assume a log-law behaviour for the bottom boundary layer (BBL), it is shown that such an approach yields high modelling accuracy of a laboratory swash event using the NSWEs.

It is well known that in the derivation of the NSWEs, directly from depth-averaging the Navier-Stokes equations, a so-called momentum correction factor, β, emerges, if the non-uniform velocities are considered. In the NSWEs it is assumed that $\beta = 1$. In reality $\beta > 1$ (Henderson 1966). The momentum correction factor is commonly approximated in river engineering, in which it is also referred to as the momentum coefficient or Boussinesq coefficient. For "fairly straight prismatic channels", $1.01 < \beta < 1.12$ (Chow 1959). In pipe flow it is also encountered: for circular pipes, $\beta = 4/3$ for laminar flow, and β depends on the friction coefficient for turbulent flow, with $\beta \approx 1.038$ for a pipe of a friction factor 0.04 (Rennels and Hudson 2012). The momentum correction factor β has also been considered when trying to reduce numerical oscillations at shocks (Yang et al. 2018).

Hogg and Pritchard (2004) derived asymptotic and similarity solutions to some gravity-driven flows in which, however, drag dominates at the leading edge. Most relevant to the swash was the dam-break flow, commonly regarded as an analogue of swash uprush. They demonstrate analytically that if flow non-uniformity exists (in which case $\beta > 1$), which we expect physically, then drag must be considered at the tip to obtain physically plausible solutions. Although they explicitly consider β in their solutions, they assume constant values $(1 - 1.2)$, corresponding to physically reasonable velocity variations in the vertical. Baldock et al. (2014), who also consider a gravity-driven flow with a leading edge, calculate values of β for a family of power-law profiles, including the turbulent flow $1/7$ power law profile for which $\beta = 1.016$.

In the numerical modeling of swash events using the NSWEs, the momentum correction factor does not appear to have been considered before. Here, we investigate the effect of this factor in modeling of swash flows. The use of the log-law BBL sub-model allows us to calculate β for swash flows, as described by the modified NSWEs so as to accommodate $\beta(x, t) > 1$ and to examine its effect. It has been pointed out (Baldock et al. 2014; Baldock and Torres-Freyermuth 2020; Zhu et al. 2022) that the boundary layer is well or fully developed in the swash tip during the uprush.

Baldock and Torres-Freyermuth (2020), reproduce a swash event using a Navier-Stokes model, and examine the depth variation in the flow in the vicinity of the tip. They evaluate this variation using an expression also referred to as β, but which is different from the momentum correction factor, and which we refer to here as β'. The β' values calculated from the numerical results indicate a fairly constant degree of deviation from a depth-invariant flow (with deviation consistent with a $1/3$ power law vertical variation, for which $\beta = 1.067$ (Baldock et al. 2014)), except very near to the tip, indicating that we may expect analogous behaviour of the momentum correction factor as it varies in space. This implies a modest deviation from the classical NSWEs, and sometimes a larger deviation in the vicinity of the tip, because of a larger momentum correction factor there, for some swash phases. This may have relevance to NSWE modelling of such flows on non-erodible and erodible beaches / structures.

In this paper we therefore use the model of Zhu et al. (2022) to directly calculate β for a swash flow as it varies in space and time. We examine the effect of incorporating β thus calculated into the numerical simulation of the swash event. As such, we make use of the vertical structure of the flow supplied by the log-law boundary layer and free flow region to evaluate β, and thereby examine its influence on the flow and on coastal engineering predictions. In open channel flows, a roughly equivalent approach has been reported by Duan (2004), in which the nonuniform velocity in the vertical direction is considered through an extra, dispersion term, instead of a coefficient. We use the experimental study by Kikkert et al. (2012), which provides measurements of a swash flow and boundary layer profile of a bore-driven swash event, to investigate the effects of the momentum correction factor.

The rest of the paper is organised as follows. In § 2, we derive and present the model equations. The numerical method to solve the equations is introduced in § 3. We then simulate the (Kikkert et al. 2012) swash event in § 4. Finally, we draw our conclusions in § 5.

GOVERNING EQUATIONS

The NSWEs including bed shear stress are utilised to describe the flow. The sub boundary layer model developed by Zhu et al. (2022) is included to simulate the flow inside the boundary layer, and calculate bed shear stresses. This allows the momentum correction factor to be calculated from the vertical flow structure obtained from the sub boundary layer model.

The modified NSWEs

The NSWEs including the momentum correction factor β can be derived from Navier-Stokes equations, the derivation process of which is not presented herein. The modified NSWEs including bottom shear stress in conservative form are

$$\frac{\partial h}{\partial t} + h\frac{\partial u}{\partial x} + u\frac{\partial h}{\partial x} = 0, \tag{1}$$

$$\frac{\partial (hu)}{\partial t} + \frac{\partial (\beta h u^2)}{\partial x} + gh\frac{\partial h}{\partial x} + gh\frac{\partial B}{\partial x} = -\frac{\tau_b}{\rho}, \tag{2}$$

where x (m) represents cross-shore distance, t (s) is time, h (m) represents water depth, u ($\mathrm{ms^{-1}}$) is a depth-averaged horizontal velocity, ρ ($\mathrm{kgm^{-3}}$) is water density, τ_b ($\mathrm{kgm^{-1}s^{-2}}$ or $\mathrm{Nm^{-2}}$) is shear stress at the bed, $B = B(x)$ (m) is the bed level (here considered as a function of x), β is the momentum correction factor, and g ($\mathrm{ms^{-2}}$) is gravitational acceleration. Note that $\beta \geq 1$, and the equal sign occurs when the flow is uniform in vertical direction.

The non-conservative form of the momentum equation is

$$\frac{\partial u}{\partial t} + (2\beta - 1)u\frac{\partial u}{\partial x} + (\beta - 1)\frac{u^2}{h}\frac{\partial h}{\partial x} + u^2\frac{\partial \beta}{\partial x} + g\frac{\partial h}{\partial x} + g\frac{\partial B}{\partial x} = -\frac{\tau_b}{\rho h}. \tag{3}$$

The non-conservative form of the mass equation is unchanged, and therefore Eqs. (1) and (3) constitute the non-conservative NWSEs.

Sub boundary layer model

The sub boundary layer model in this work is based on Zhu et al. (2022, Briganti et al. (2011, Fredsøe and Deigaard (1993), and the spatial gradients in velocity and boundary layer thickness are taken into consideration.

The horizontal velocity in the vertical direction of the water column is denoted by $U(x, z, t)$.

The horizontal velocity inside the boundary layer is approximated using the logarithmic law

$$U(x, z \leq z_0 + \delta, t) = \frac{U_f}{\kappa} \ln\left(\frac{z}{z_0}\right), \tag{4}$$

where z (m) is the vertical distance from the bed, $\kappa = 0.4$ is von Karman's constant, and z_0 (m) is the vertical distance from the bed at which the velocity is assumed to be 0, and here $z_0 = K_n/30$ with K_n being the bed roughness. U_f is the friction velocity,

$$U_f = U_f(x, t) = \frac{U_0}{|U_0|}\sqrt{|\ \tau_b\ |\ /\rho}, \tag{5}$$

where U_0 is free stream velocity, which is the flow velocity outside the boundary layer. At the upper limit of the boundary layer where $z = z_0 + \delta$ with δ the boundary layer thickness,

$$U(x, z = z_0 + \delta, t) = U_0 = \frac{U_f}{\kappa} \ln\left(\frac{z_0 + \delta}{z_0}\right) = \frac{U_f}{\kappa} Z \tag{6}$$

where $Z = \ln\left(\frac{\delta + z_0}{z_0}\right)$. Thus, $U_f = \frac{U_0 \kappa}{Z}$.

The momentum equation for the flow outside the boundary layer is

$$\frac{\partial U_0}{\partial t} + U_0 \frac{\partial U_0}{\partial x} = -g\frac{\partial h}{\partial x} - g\frac{\partial B}{\partial x}, \tag{7}$$

and that for the flow inside the boundary layer is

$$\frac{\partial U}{\partial t} + U\frac{\partial U}{\partial x} = -g\frac{\partial h}{\partial x} - g\frac{\partial B}{\partial x} + \frac{1}{\rho}\frac{\partial \tau}{\partial z} \tag{8}$$

where $\tau = \tau(x, z, t)$ is shear stress at location (x,z) at time t.

Subtracting Eq. (7) from Eq. (8) gives

$$\frac{\partial}{\partial t}(U_0 - U) + \frac{\partial}{\partial x}\left(\frac{1}{2}U_0^2 - \frac{1}{2}U^2\right) = -\frac{1}{\rho}\frac{\partial \tau}{\partial z}. \tag{9}$$

Integrating Eq. (9) across the boundary layer $[z_0, z_0 + \delta]$ gives

$$\frac{\tau_b}{\rho} = \int_{z_0}^{z_0+\delta} \frac{\partial}{\partial t}(U_0 - U)dz + \int_{z_0}^{z_0+\delta} \frac{\partial}{\partial x}\left(\frac{1}{2}U_0^2 - \frac{1}{2}U^2\right)dz, \tag{10}$$

Using Eq. (4) and the definition of U_f from Eq. (5) we then arrive at a differential equation for Z from Eq. (10):

$$\frac{\partial Z}{\partial t} + \frac{U_0}{f_2 Z}\left(f_1 + f_2(Z-1)\right)\frac{\partial Z}{\partial x} = \frac{\kappa^2}{z_0 f_2}|U_0| - \frac{f_1 Z}{f_2 U_0}\frac{\partial U_0}{\partial t} - \frac{(f_2 + f_1(Z-1))}{f_2}\frac{\partial U_0}{\partial x}, \tag{11}$$

where $f_1 = e^Z - Z - 1$ and $f_2 = Ze^Z - e^Z + 1$. Eq. (11) is solved to get Z, from which δ and U_0 can be obtained, and so the flow inside the boundary layer is known. The bed shear stress can further be calculated by

$$\tau_b = \rho U_f^2 = \rho\kappa^2\frac{U_0^2}{Z^2}. \tag{12}$$

Note that the bed shear stress $\tau_b \to \infty$ for the boundary layer thickness $\delta \to 0$, i.e., $Z \to 0$, which gives an unbounded friction coefficient $c_d = \frac{|\tau_b|}{\rho u^2}$. We follow Zhu et al. (2022) and impose the maximum friction coefficient of $c_d = 0.0597$ under these circumstances to limit the bed shear stress. For further details of the sub boundary layer model the reader is referred to Zhu et al. (2022).

Derivation of the momentum correction factor β

The depth-averaged velocity is

$$u = \frac{1}{h}\int_{z_0}^{h+z_0} U dz. \tag{13}$$

When $\delta < h$,

$$u = \frac{1}{h}\int_{z_0}^{h+z_0} U dz = \frac{1}{h}\left\{U_0(h+z_0) - \frac{U_f}{\kappa}\delta\right\} \tag{14}$$

$$\beta = \frac{\int_{z_0}^{h+z_0} U^2 dz}{hu^2} = \frac{h\left\{(h+z_0) - 2\frac{z_0+\delta}{Z} + 2\frac{\delta}{Z^2}\right\}}{\left(h + z_0 - \frac{\delta}{Z}\right)^2} \tag{15}$$

In the limit of $h \to 0$, $\delta \to 0$ but $\delta < h$. The limiting value of β as $h \to 0$ is derived in Appendix I, and it depends on the ratio between δ and h, i.e., $\frac{\delta}{h}$.

If the boundary layer is allowed to grow without limits, $\delta \geq h$ would occur, but we set $\delta = h$, so that the boundary layer terminates at the water surface and $U_0 = U(x, z = h, t)$. In this case we get:

$$u = \frac{1}{h}\int_{z_0}^{h+z_0} U dz = \frac{1}{h}\left\{U_0(h+z_0) - \frac{U_f}{\kappa}h\right\} \tag{16}$$

$$\beta = h\frac{(h+z_0)\ln^2(1+\frac{h}{z_0}) - 2(h+z_0)\ln(1+\frac{h}{z_0}) + 2h}{((h+z_0)\ln(1+\frac{h}{z_0}) - h)^2}. \tag{17}$$

The limiting value of β as $h \to 0$ is also derived in Appendix I, and it shows that when $h = 0$, $\beta = \frac{4}{3}$. This value is the same as the momentum correction factor for laminar flow in circular pipes. In this limit we regard the boundary layer as being fully developed at the tip.

NUMERICAL METHOD

The Specified Time Interval Method of Characteristics (STI-MOC) method is used to solve the equations.

Riemann equation and characteristics

The combination of Eqs. (1) and (3) gives the following Riemann equations

$$\frac{\lambda - (2\beta - 1)u}{h}\frac{dh}{dt} + \frac{du}{dt} = -u^2\frac{\partial \beta}{\partial x} - g\frac{\partial B}{\partial x} - \frac{\tau_b}{\rho h} \tag{18}$$

$$\text{along} \quad \frac{dx}{dt} = \lambda = u\beta \pm \sqrt{\beta(\beta-1)u^2 + gh} \tag{19}$$

from which we can see that the inclusion of β would alter the Riemann equations, and the characteristics λ. Note that for $\beta = 1$, the two characteristics $\lambda^{\pm} = u \pm \sqrt{gh}$ are recovered. We use $\lambda^{\pm}$ to refer to the equivalent two roots in Eq. (19).

Shock conditions

Applying the mass and momentum conservation across a shock, i.e., a bore, gives the Rankine-Hugoniot conditions:

$$-W(h_R - h_L) + (h_R u_R - h_L u_L) = 0, \tag{20}$$

$$\begin{aligned} -W(h_R u_R - h_L u_L) + \left(\beta_R h_R u_R^2 + \frac{1}{2} g h_R^2 - \beta_L h_L u_L^2 - \frac{1}{2} g h_L^2\right) \\ + \frac{1}{2} g (h_R + h_L)(B_R - B_L) = 0, \end{aligned} \tag{21}$$

where the subscripts L and R represent the left and right sides of the shock, W is the shock velocity. Note that these are identical to those of Hogg and Pritchard (2004), but written here in more conventional form, and here including variations in bed level.

Wet-dry boundary

At the tip $h = 0$,

$$\lambda^{\pm} \quad = \quad u\beta \pm \sqrt{\beta(\beta - 1)u^2}. \tag{22}$$

Note that for $\beta > 1$, the two characteristics $\lambda^+ \neq \lambda^-$ with $\lambda^+ > u$ and $\lambda^- < u$, which are different from the $\beta = 1$ case. However, the shoreline moves at u, which can be derived from Eq. (20).

When the boundary layer occupies the whole water column, substituting $\beta = \frac{4}{3}$ at the shoreline gives

$$\lambda^+ = 2u \qquad \text{and} \qquad \lambda^- = \frac{2}{3}u \quad \text{in uprush with } u > 0; \tag{23}$$

$$\lambda^+ = \frac{2}{3}u \qquad \text{and} \qquad \lambda^- = 2u \quad \text{in backwash with } u < 0. \tag{24}$$

The Riemann equation along the λ^+ characteristic can be used to solve for u at the shoreline because $\lambda^+ > u$ and the characteristic line extends from the interior flow to the shoreline. However, the Riemann equation along λ^- cannot be used because $\lambda^- < u$, and the characteristic line goes back to the dry region. However, extrapolation is used for the approximation of u at the shoreline due to the singular problem of zero depth.

APPLICATION TO THE SWASH EVENT OF KIKKERT ET AL. (2012)

The experiment of a dam-break swash event on a rough, impermeable, immobile beach carried out by Kikkert et al. (2012) in the laboratory, which was considered by Briganti et al. (2011) and Zhu et al. (2022), is utilised in this work to investigate the momentum correction factor. These measurements allow a detailed comparison against h, u and x_s (shoreline position), as well as the vertical structure of the flow for a bore-driven swash, which is not usually available, and this allows a direction calculation of β. The motivation is to evaluate the performance of the model in which β is calculated from Eq. (17) against one in which it is assumed that $\beta = 1$.

For the initial set up of the Kikkert et al. (2012) experiment, the reader is referred to Zhu et al. (2022). The beach consists of a flat part, and a sloping part of slope 1/10. The roughness of the sloping section is determined by the sediment affixed to it. The water depth in the reservoir is 0.6 m, and the initial water depth in front of the gate is 0.062 m.

The IMP015 case is considered (Briganti et al. 2011; Zhu et al. 2022), in which $D_{50} = 1.3$ mm. The bed roughness $K_n = 2D_{65} = 3$ mm is estimated using the Engelund and Hansen (1967) formula, which was selected by Briganti et al. (2011) due to its providing consistently small discrepancies with measurements compared to other available definitions. We follow Briganti et al. (2011, Zhu et al. (2022) in driving the simulation by the measured water depths h and depth-averaged velocities u at PIV 1.

Comparison with measurements

As was pointed out in § 3, the inclusion of β yields a number of changes, both in the Riemann equations Eq. (18), and the characteristics λ Eq. (19). Accordingly, in our comparison we examine separately the effect of: (a) including both the modified characteristics and Riemann equations; (b) including only the modified characteristics (i.e. assuming $\beta = 1$ in the Riemann equations); (c) including only the modified Riemann equations (i.e. assuming $\beta = 1$ in the characteristics); (d) including only the modified Riemann equations (i.e. assuming $\beta = 1$ in the characteristics) but omitting the term involving $\frac{\partial \beta}{\partial x}$ (i.e., assuming $\beta = 1$ for that term). We also compare these against the model of Zhu et al. (2022), for which $\beta = 1$.

Shoreline movement

The comparison between the numerical and the measured shoreline trajectories is shown in Fig. 1. In the experiment, the shoreline is located where $h = 0.005$ m. The measured shoreline movement for $h = 0.005$ m is very well captured by the model with $\beta = 1$ as already shown in Zhu et al. (2022). The inclusion of the momentum correction factor β, in various forms, results in larger discrepancies.

These discrepancies are quantified in Table 1. The Root Mean Squared Error (RMSE) of numerical shoreline positions vs the measured results is calculated from

$$\text{RMSE}_{xs} = \sqrt{\frac{\sum_{i=1}^{N_{xs}} (x_{s,mi} - x_{s,ni})^2}{N_{xs}}} \tag{25}$$

where N_{xs} is the number of points of measured shoreline position $x_{s,m}$, $x_{s,mi}$ is the ith measured shoreline position, and $x_{s,ni}$ is the ith modelled shoreline position.

Fig. 1 shows that for case (a), for which both modified characteristics and Riemann equations are included (blue line), the shoreline position (x_s) is generally overestimated. If only the modified characteristics are included (b), modelling deteriorates overall further (see also Table 1), although the maximum run-up is slightly closer to the measured value. In this case x_s is underestimated. For (c), only modified Riemann equations, there is a further deterioration, but now with an additional overestimation of x_s compared to (a). Case (b) ((c)) tells us that the effect of including the modified characteristics (Riemann equations) is to reduce (increase) the modelled run-up. Finally, we can see the effect of the $\frac{\partial \beta}{\partial x}$ term in case (d), which also considers only the Riemann equations but neglect $\frac{\partial \beta}{\partial x}$ (set $\frac{\partial \beta}{\partial x} = 0$). Comparison with (c) shows that the effect of the $\frac{\partial \beta}{\partial x}$ term is to reduce run-up.

Table 1 and Fig. 1 reveal that case (a), which in theory one would expect to be the most complete description of the dynamics, gives inferior modelling of x_s to the modelling with $\beta = 1$ (Zhu et al.

2022). This might imply that the velocity profile in the boundary layer is, at least in some regions, not well described by the logarithmic law. The deviations of the numerical boundary layer from the log-profile were discussed by Baldock and Torres-Freyermuth (2020).

Spatial variation

The comparison of the snapshots of B and η (free surface level, i.e., $B + h$), u and β are shown in Figs. 2-4, respectively. The discrepancy in free surface η mainly occurs in the tip region, and is most evident in the uprush (see the blue and red lines in the first four subfigures); the run-up is generally larger when $\beta \neq 1$, consistent with Fig. 1. The only significant discrepancy in the boundary layers is very early in the uprush ($t = 2.44$ s), where the $\beta = 1$ boundary layer is less well developed. This implies a larger bed shear stress early in the swash event for $\beta = 1$. In Fig. 3 we show the equivalent depth-averaged velocity plots (no measurements are available for comparison here). Again, early in the swash event the main difference is in the tip region. This region expands as the swash event unfolds, which is consistent with the initial differences. This yields slightly enhanced run-up for $\beta \neq 1$, also resulting in slightly enhanced backwash. Finally, in Fig. 4 we show the equivalent plots for β. We can see ($\beta \neq 1$) that for most of the uprush $\beta \approx 1.02$ except very near to the tip, where β increases rapidly, and ($t = 3.41$ s) $\longrightarrow 4/3$, resulting in a large $\frac{\partial \beta}{\partial x}$ very near to the tip. This value of β away from the tip is similar to that from a $1/7$ power law profile (Baldock et al. 2014). In the backwash, the gradient at the tip in β is reduced, and at the tip we similarly have $\beta = 4/3$. In the early uprush, $\beta < 4/3$ at the tip showing that the boundary layer is not fully developed very near the tip when $\beta \neq 1$.

However the boundary layer upper limit is very close to the free surface at the tip, and the boundary layer thickness grows to the free surface further away from the tip (Fig. 2).

Figures 2-4 also help to illustrate the effects of β in bore-driven swash flows. Fig. 4 indicates that for these flows $1 < \beta \leq 4/3$, but that at most locations / times away from the tip β is much smaller: see Table 2, in which the average β is calculated at each time. The average of all these values is 1.04.

Furthermore, $\frac{\partial \beta}{\partial x}$ is very small away from the swash tip, at which location the gradient is always positive. So, if we write

$$\beta = 1 + \epsilon \quad \text{where} \quad \epsilon \ll 1 \quad \text{(usually)}$$

we can rewrite the terms in the momentum equation (3) so as to explicitly express the extra contributions due to a varying β as

$$\frac{\partial u}{\partial t} + u\frac{\partial u}{\partial x} + 2\epsilon u\frac{\partial u}{\partial x} + \epsilon\frac{u^2}{h}\frac{\partial h}{\partial x} + u^2\frac{\partial \epsilon}{\partial x} + g\frac{\partial h}{\partial x} + g\frac{\partial B}{\partial x} = -\frac{\tau_b}{\rho h}, \tag{26}$$

with

$$\text{enhanced advective acceleration:} \qquad 2\epsilon u\frac{\partial u}{\partial x}, \tag{27}$$

$$\beta \ \text{gradient:} \qquad u^2\frac{\partial \epsilon}{\partial x}, \tag{28}$$

$$\text{enhanced pressure gradient:} \qquad \epsilon\frac{u^2}{h}\frac{\partial h}{\partial x}. \tag{29}$$

It can be seen that in the uprush there is an additional component of the advective acceleration term (27). If viewed as an enhanced acceleration term, then, because the gradient in u is mostly positive in the uprush, this contribution will act to reduce u (because the same forcing will equate to a smaller acceleration). Very near the tip, however, the negative gradient in u (Fig. 3) may yield a locally increased shoreline velocity.

The β gradient term (28) also emerges from the advective acceleration term. It will clearly be positive but small, except very near the tip, where it will be positive and large (Fig. 4). So, this term will act to reduce u in the vicinity of the tip, thus opposing the effect of (27) there.

In most of the uprush the enhanced pressure gradient term (29) is likely to increase run-up. Only early in the swash event and at the tip in the uprush is $\frac{\partial h}{\partial x} < 0$ (onshore directed) (Fig. 2). In this vicinity we have a small h, a large u and a large β. So, there will be a significant additional onshore force at the tip, acting to increase run-up.

The overall balance in these terms is shown in Fig. 5, in which these terms are normalised by the maximum of the magnitude of non-ϵ terms in Eq. (26) at each time over all x. At the very tip in the uprush it is apparent that the sum of the ϵ terms are of similar magnitude to the maximum non-ϵ term magnitude indicating the significant impact of ϵ terms. It is also clear that the enhanced run-up in the $\beta \neq 1$ model is due primarily to the enhanced pressure gradient term (29), which overcomes the β gradient advective acceleration term (28).

In the backwash these terms are negligible or oppose each other (note that the very large values near the base of the backwash are due to differentiation across a backwash bore, which therefore have no significance). This implies that the discrepancies observed in the late backwash are a result of the earlier ones at the swash tip in the uprush.

Time series

The comparison of the time series at PIV 2, 4, and 5, the locations of which are at $x = 0.072$ m, 1.559 m and 2.365 m, respectively, are shown in Fig. 6. Once again, the RMSE values are calculated, for water depth and velocity:

$$\mathrm{RMSE}_h = \sqrt{\frac{\sum_{i=1}^{N_h}(h_{mi} - h_{ni})^2}{N_h}},$$

$$\text{and} \quad \mathrm{RMSE}_u = \sqrt{\frac{\sum_{i=1}^{N_u}(u_{mi} - u_{ni})^2}{N_u}} \tag{30}$$

where N_h (N_u) is the number of points of measured water depths h_m (velocities u_m), h_{mi} (u_{mi}) is the ith measured water depth (velocity), and h_{ni} (u_{ni}) is the ith modelled water depth (velocity). The RMSE values are shown in Table 3.

Comparison with these measurements shows a trend similar to the shoreline comparison in that the $\beta = 1$ model displays closer agreement with the data, but here the errors in both models are small, especially for h. And there is generally closer agreement between the two modelling approaches lower in the swash than in the upper swash, although the errors both decrease in the upper swash. This is consistent with the shoreline plot. The errors at PIV 2-5 also indicate that much of the inaccuracy in the modelling is indeed at the tip.

Velocity profile in the boundary layer

The velocity profiles are compared against the measured velocities in Fig. 7. The boundary layers for $\beta = 1$ and $\beta \neq 1$ are mostly similar. In this comparison the discrepancy between measurements and either model is most apparent. The detailed measurements obtained by Kikkert et al. (2012) allow us to calculate β directly from the measurements at each time, and compare those values against the ones from the $\beta \neq 1$ model, and also to post-calculate β values from the BBL profiles for the $\beta = 1$ model as shown in Fig. 8(a). The measured and modelled β values are larger at inundation and also when the flow becomes thin in the backwash. The β values from the measurements show reasonable correspondence with numerical values in the uprush, except at the swash tip, and also in the backwash, diverging in the late backwash. The variation of β in time in Fig. 8(a) is consistent with the spatially averaged β values shown in Table 2. Finally, in Fig. 8(b) we plot $\beta' = \frac{1}{u}\sqrt{\frac{1}{h}\int_{z_0}^{z_0+h}(U(x,z,t)-u(x,t))^2}$ at different times (Baldock and Torres-Freyermuth 2020) in the uprush, 1 m from the swash tip Baldock and Torres-Freyermuth (2020). This shows a roughly similar picture of the degree of and variation in depth uniformity of velocity in the uprush, as in the Navier-Stokes modelling of Baldock and Torres-Freyermuth (2020), except with most β' values between about $0.2 - 0.1$, with the latter value in the early uprush only. Toward the tip there is a general increase, especially at the tip. Experimental values are roughly consistent, but toward the lower end of the range. The schematized flow vertical structure therefore appears to reproduce observed / modelled variation reasonably accurately, except very near to the tip of the uprush.

CONCLUSIONS

The expression for the momentum correction factor β, which is a measure of the degree to which the horizontal velocity in water column deviates from the depth-averaged velocity, is derived by use of the log-law boundary layer, and included in a model based on NSWEs for the swash zone such that β can be calculated. The swash event of Kikkert et al. (2012) is simulated by the resulting model.

The inclusion of time- and space-varying β has a small impact on the overall swash flow but a significant impact on the shoreline movement. This is because of the increased onshore-directed force at the swash tip in the uprush due to the enhanced pressure gradient there. Overall, therefore, the agreement between the new model (i.e. for $\beta \neq 1$) with the measured data is slightly worse–a larger over-prediction of the shoreline position–than the agreement between the same data and the model of Zhu et al. (2022), which utilises the same BBL sub-model, but in which it is assumed that $\beta = 1$. Similarly, velocity magnitudes in the late backwash are slightly more over-predicted, which appears to be a result of the aforementioned initial over-prediction.

The predicted values of β are consistent with other shallow water flows. They are generally very small away from the swash tip (~ 1.02 in the uprush; $\sim 1.02 - 1.1$ in the backwash). Values of β generally gradually increase toward the tip with a rapid increase to $4/3$ at the tip. These trends are reproduced in the data of Kikkert et al. (2012), but with typical values somewhat larger near flow reversal $(1.05 - 1.12)$ and in the late backwash $(1.05 - 1.1)$, and smaller at the tip. A similar picture is revealed by examining β' in the uprush, following Baldock and Torres-Freyermuth (2020). Thus, the BBL sub-model provides a qualitative and quantitatively reasonable picture of the vertical variation on velocity in the swash.

So, it appears that the reason for the slightly worse performance of the $\beta \neq 1$ model vs the standard ($\beta = 1$) model is connected to the swash tip. However, allowing β to vary realistically should, in principle, yield a more accurate description of the dynamics (because in reality $\beta \neq 1$). So, this slightly deteriorated predictive capability is curious. This observed deterioration in modelling at the swash tip, in an otherwise accurate NSWEs-based simulation, implies that this deterioration is a consequence of the use of the log-law boundary layer at the tip. In the $\beta = 1$ model, the use of the log-law only has consequences for the calculation of bed shear stress, τ_b. However, the non-depth-uniformity in the flow that this use implies has more fundamental consequences in the vicinity of the tip, which we see in the $\beta \neq 1$ model. This therefore implies that in the vicinity of the tip the log-law sub-model is not an accurate description of the flow there, in particular because of vertical fluid motions in this region (Baldock et al. 2014). The Navier-Stokes simulations of Baldock and Torres-Freyermuth (2020) also imply a different structure at the swash tip, at least in the uprush. This, and the similarity of the log-law profile to related power law profiles (Baldock et al. 2014; Hogg and Pritchard 2004), seem to imply the need for a qualitatively different flow sub-model at the tip.

Lastly, as noted, the $\beta = 1$ model gives satisfactory modelling, so from an engineering standpoint it could perhaps be argued that we do not need the $\beta \neq 1$ model. However, it seems to the authors that it points to a more fundamental deficiency in NSWE modeling, which is likely to manifest itself in particular in estimates of bed shear stress at the swash tip. Present practice is usually to cap this value at an ad hoc figure. However, this will be case dependent, as well as inherently unsatisfactory, especially because the largest bed shear stresses in the swash are exerted at the swash tip in the uprush (Kikkert et al. 2012; Baldock and Torres-Freyermuth 2020). So, we are likely to need a fuller description to make more reliable engineering predictions, especially when considering morphodynamics and bed change. The present work therefore points the way forward in consideration of a possible augmentation to the NSWE plus BBL sub-model approach in the form of a different sub-model in the tip region. The work of Baldock et al. (2014) provides a possible schematized sub-model for the tip region. To test the efficacy of such a model a different data-set to that used here would be ideal.

Data Availability Statement

All data, models, or code that support the findings of this study are available from the corresponding author on reasonable request.

Acknowledgments

This work is supported by Natural Science Foundation of China (project code 51811530012) and The Swedish Foundation for International Cooperation In Research and Higher Education (project code CH2017-7218). Their support is gratefully acknowledged. We are grateful to the comments and suggestions of Professor Tom Baldock, and two anonymous reviewers.

APPENDIX I. THE LIMITING VALUE OF β AS $H \to 0$ FOR $\delta = H$ AND $\delta < H$

In the limit of $h \to 0$ for $\delta = h$,

$$
\begin{aligned}
\beta &= h\frac{(h+z_0)Z^2 - 2(h+z_0)Z + 2h}{((h+z_0)Z - h)^2} \\
&= h\frac{(h+z_0)\ln^2\left(1+\frac{\delta}{z_0}\right) - 2(h+z_0)\ln\left(1+\frac{\delta}{z_0}\right) + 2h}{\left((h+z_0)\ln\left(1+\frac{\delta}{z_0}\right) - h\right)^2} \\
&= h\frac{(h+z_0)\ln^2\left(1+\frac{h}{z_0}\right) - 2(h+z_0)\ln\left(1+\frac{h}{z_0}\right) + 2h}{\left((h+z_0)\ln\left(1+\frac{h}{z_0}\right) - h\right)^2} \\
&= \frac{h}{z_0}\frac{\left\{\left(1+\frac{h}{z_0}\right)\ln^2\left(1+\frac{h}{z_0}\right) - 2\left(1+\frac{h}{z_0}\right)\ln\left(1+\frac{h}{z_0}\right) + 2\frac{h}{z_0}\right\}}{\left\{\left(1+\frac{h}{z_0}\right)\ln\left(1+\frac{h}{z_0}\right) - \frac{h}{z_0}\right\}^2}
\end{aligned}
\tag{31}
$$

When $\frac{h}{z_0} \to 0$,

$$
\ln\left(1+\frac{h}{z_0}\right) \approx \frac{h}{z_0} - \frac{1}{2}\frac{h^2}{z_0^2} + \frac{1}{3}\frac{h^3}{z_0^3} \tag{32}
$$

Substituting (32) into (31) gives

$$
\begin{aligned}
\beta &= \frac{h}{z_0}\frac{\frac{1}{3}\frac{h^3}{z_0^3} + O(\frac{h^4}{z_0^4})}{\frac{1}{4}\frac{h^4}{z_0^4} + O(\frac{h^5}{z_0^5})} \\
&= \frac{4}{3}.
\end{aligned}
\tag{33}
$$

For $\delta < h$, we assume that in the limit $h \to 0$, we can write:

$$
\delta \sim \sigma h \quad \text{as} \quad h \to 0 \quad \text{for} \quad \sigma < 1 \tag{34}
$$

where σ is yet to be determined.

It is obtained that in the limit $h \longrightarrow 0$

$$\beta = \frac{(1-\frac{2}{3}\sigma)}{(1-\frac{1}{2}\sigma)^2} \tag{35}$$

β varies between 1 and $\frac{4}{3}$ for $0 \leq \sigma \leq 1$.

Note that when $\delta < h$,

$$\tau_b = \rho\kappa^2 \frac{h^2 u^2}{\{Z\,(z_0+h)-\delta\}^2}. \tag{36}$$

If we take $h \longrightarrow n z_0$ at the tip,

$$\tau_b = \rho\kappa^2 \frac{n^2}{\{(1+n)\ln(1+\delta/z_0)-\delta/z_0\}^2} u^2. \tag{37}$$

Now, if we assume that $\delta = \sigma h = \sigma n z_0$ (34), we get:

$$\tau_b = \rho\kappa^2 \frac{n^2}{\{(1+n)\ln(1+\sigma n)-\sigma n\}^2} u^2. \tag{38}$$

as $h \longrightarrow 0$. The bed shear stress in this case is larger than the equivalent but with $\delta = h$.

β' for the logarithmic boundary layer

For a logarithmic boundary layer extending to the free surface $\frac{U}{u_s} = \frac{\ln\left(\frac{z}{z_0}\right)}{\ln\left(1+\frac{h}{z_0}\right)}$, and after some algebra we get:

$$\beta' = \left\{ \frac{1-\frac{z_0}{h}\left(\frac{z_0}{h}+1\right)Z^2}{\left(\frac{z_0}{h}+1\right)^2 Z^2 - 2\left(\frac{z_0}{h}+1\right)Z + 1} \right\}^{1/2}. \tag{39}$$

REFERENCES

Baldock, T. E. (2018). “"Bed shear stress, surface shape and velocity field near the tips of dam-breaks, tsunami and wave runup" by Peter Nielsen.” Coastal Eng., 142, 77–81.

Baldock, T. E., Grayson, B., Torr, B., and Power, H. (2014). “Flow convergence at the tip and edges of a viscous front – experimental and analytical modelling.” Coastal Eng., 88, 123–130.

Baldock, T. E. and Torres-Freyermuth, A. (2020). “Numerical study of the flow structure at a swash tip propagating over a rough bed.” Coastal Eng., 161, 103729.

Barnes, M. P. and Baldock, T. E. (2010). “A Lagrangian model for boundary layer growth and bed shear stress in the swash zone.” Coastal Eng., 57, 385–396.

Briganti, R., Dodd, N., Pokrajac, D., and O’Donoghue, T. (2011). “Non linear shallow water modelling of bore-driven swash: Description of the bottom boundary layer.” Coastal Eng., 58(6), 463–477.

Briganti, R., Torres-Freyermuth, A., Baldock, T. E., Brocchini, M., Dodd, N., Hsu, T.-J., Jiang, Z., Kim, Y., Pintado-Patiño, J. C., and Postacchini, M. (2016). “Advances in numerical modelling of swash zone dynamics.” Coastal Eng., 115, 26–41.

Brocchini, M. and Dodd, N. (2008). “Nonlinear shallow water equation modeling for coastal engineering.” ASCE J. Water. Port Coast. Ocean Eng., 134(2), 104–120.

Chow, V. T. (1959). Open-channel hydraulics. McGraw-Hill.

Duan, J. (2004). “Simulation of flow and mass dispersion in meandering channels.” ASCE J. Hydraulic Eng., 130, 964–976.

Engelund, F. and Hansen, E. (1967). “A monograph on sediment transport.” Report no., Teknisk Forlag, Copenhagen, Denmark.

Fredsøe, J. and Deigaard, R. (1993). Mechanics of Coastal Sediment Transport, Vol. 3 of Advanced Series on Ocean Engineering. World Scientific, Singapore.

Henderson, F. (1966). Open channel flow. MacMillan.

Hogg, A. J. and Pritchard, D. (2004). “The effects of hydraulic resistance on dam-break and other shallow inertial flows.” J. Fluid Mech., 501(DOI: 10.1017/S0022112003007468), 179–212.

Incelli, G., Dodd, N., Blenkinsopp, C. E., Zhu, F., and Briganti, R. (2016). "Morphodynamical modelling of field-scale swash events." Coastal Eng., 115, 42–57.

Kikkert, G., O'Donoghue, T., Pokrajac, D., and Dodd, N. (2012). "Experimental study of bore-driven swash hydrodynamics on impermeable rough slopes." Coastal Eng., 60, 149–166.

Pintado-Patiño, J. C., Torres-Freyermuth, A., Puleo, J. A., and Pokrajac, D. (2015). "On the role of infiltration and exfiltration in swash zone boundary layer dynamics." J. Geophys. Res., 120, 6329–6350.

Puleo, J. A., Farhadzadeh, F., and Kobayashi, N. (2007). "Numerical simulation of swash zone fluid accelerations." J. Geophys. Res., 112(C7).

D. C. Rennels and H. M. Hudson, eds. (2012). Pipe flow : a practical and comprehensive guide. John Wiley & Sons, Incorporated.

Torres-Freyermuth, A., Puleo, J. A., and Pokrajac, D. (2013). "Modeling swash-zone hydrodynamics and shear stresses on planar slopes using Reynolds-Averaged Navier-Stokes equations." J. Geophys. Res., 118(2), 1019–1033.

Yang, S., Yang, W., Qin, S., Li, Q., and Yang, B. (2018). "Numerical study on characteristics of dam-break waves." Ocean Eng., 159, 358–371.

Zhu, F. and Dodd, N. (2013). "Net beach change in the swash: A numerical investigation." Advances in Water Resources, 53, 12–22.

Zhu, F. and Dodd, N. (2015). "The morphodynamics of a swash event on an erodible beach." J. Fluid Mech., 762, 110–140.

Zhu, F., Dodd, N., Briganti, R., Larson, M., and Zhang, J. (2022). "A logarithmic bottom boundary layer model for the unsteady and non-uniform swash flow." Coastal Eng., 172, 104048.

List of Tables

TABLE 1. RMSE values and maximum run-up relative error (mrre) compared to the measured shoreline, calculated from the various cases.

Case	$\beta = 1$	$\beta \neq 1$ (a)	$\beta \neq 1$ (b)	$\beta \neq 1$ (c)	$\beta \neq 1$ (d)
RMSE	0.10	0.26	0.45	0.48	0.66
mrre	0.017	0.090	−0.034	0.12	0.17

TABLE 2. Average values for β at the various time indicated in Fig 4.

t [s]	2.44	3.41	4.45	5.41	6.45	7.41	8.45	9.41
β	1.02	1.03	1.03	1.01	1.03	1.05	1.07	1.08

TABLE 3. The RMSE values of the modelled time series results of h and u at PIV 2, 4, and 5.

		h	
Simulation	PIV2	PIV4	PIV5
$\beta = 1$	1.2×10^{-2}	6.7×10^{-3}	6.3×10^{-3}
$\beta \neq 1$	1.3×10^{-2}	8.0×10^{-3}	7.8×10^{-3}
		u	
$\beta = 1$	0.15	0.11	0.073
$\beta \neq 1$	0.18	0.14	0.11

List of Figures

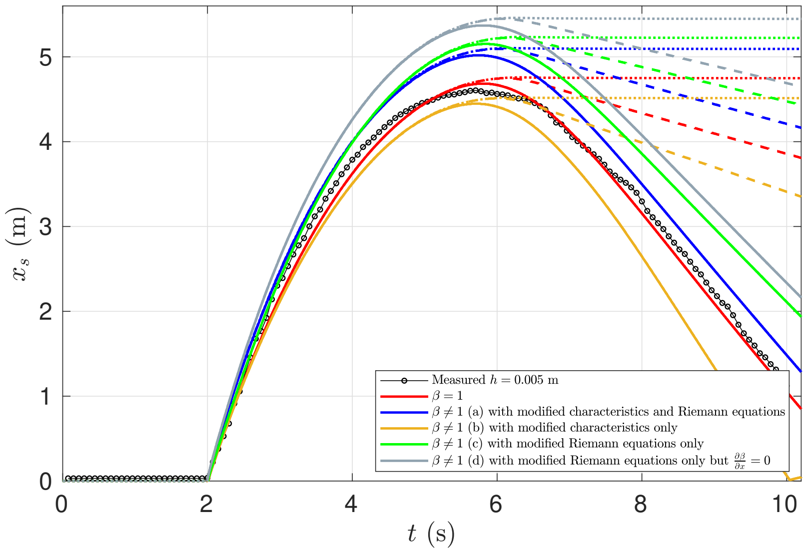

Fig. 1. The comparison between numerical and measured shoreline trajectories. Solid lines: $h = 0.005$ m; dashed lines: $h = 0.001$ m; and dotted lines: $h = 0$ m.

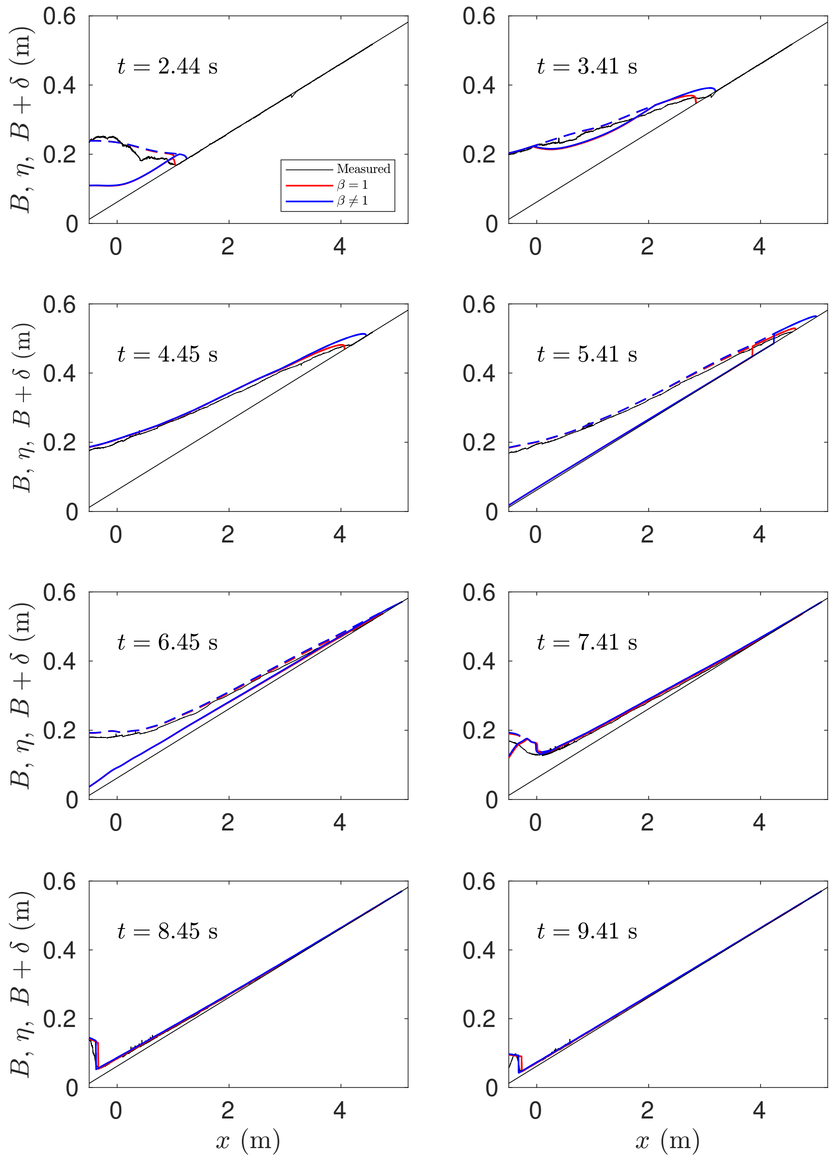

Fig. 2. Snapshots of the measured and modelled flow (B, η and $B + \delta$) at different times. Thin lines: B and measured η; thick solid lines: modelled η, and thick dashed lines: modelled $B + \delta$, which indicate the upper limits of the corresponding boundary layers.

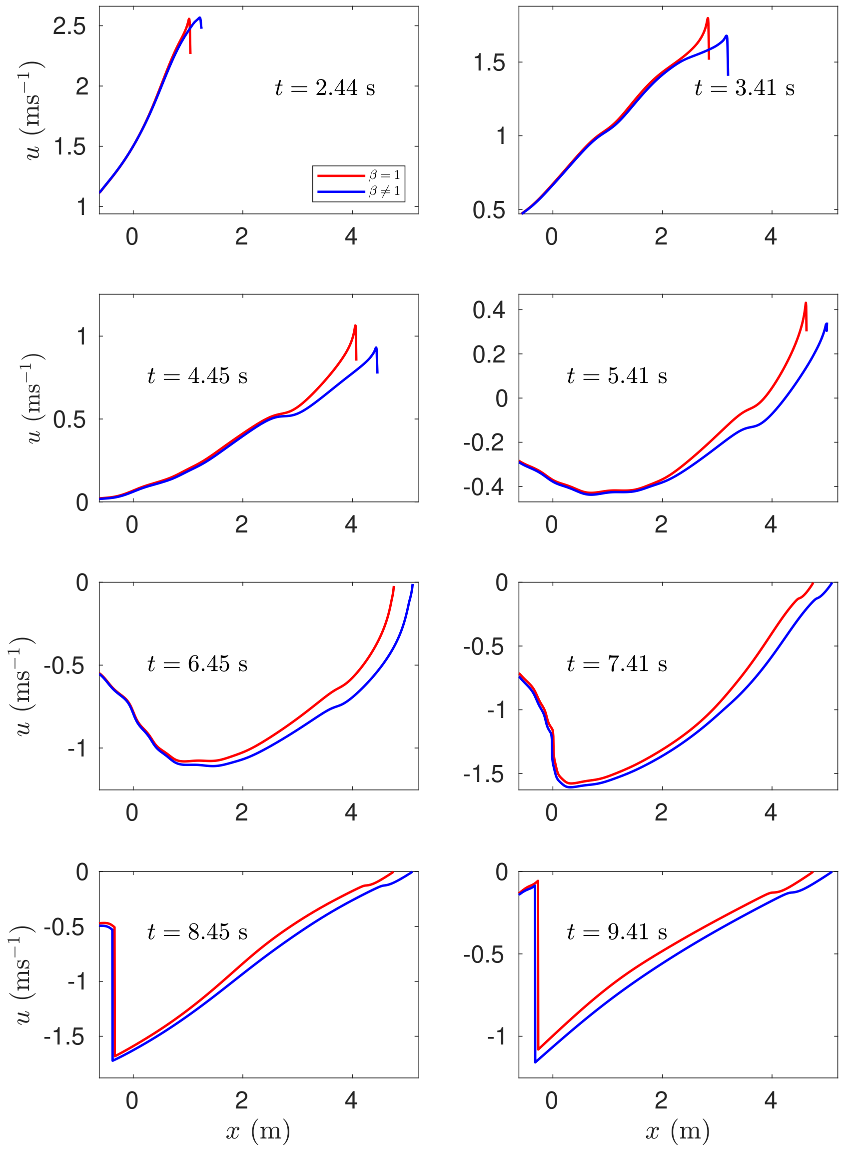

Fig. 3. Snapshots of the modelled flow (u) at different times.

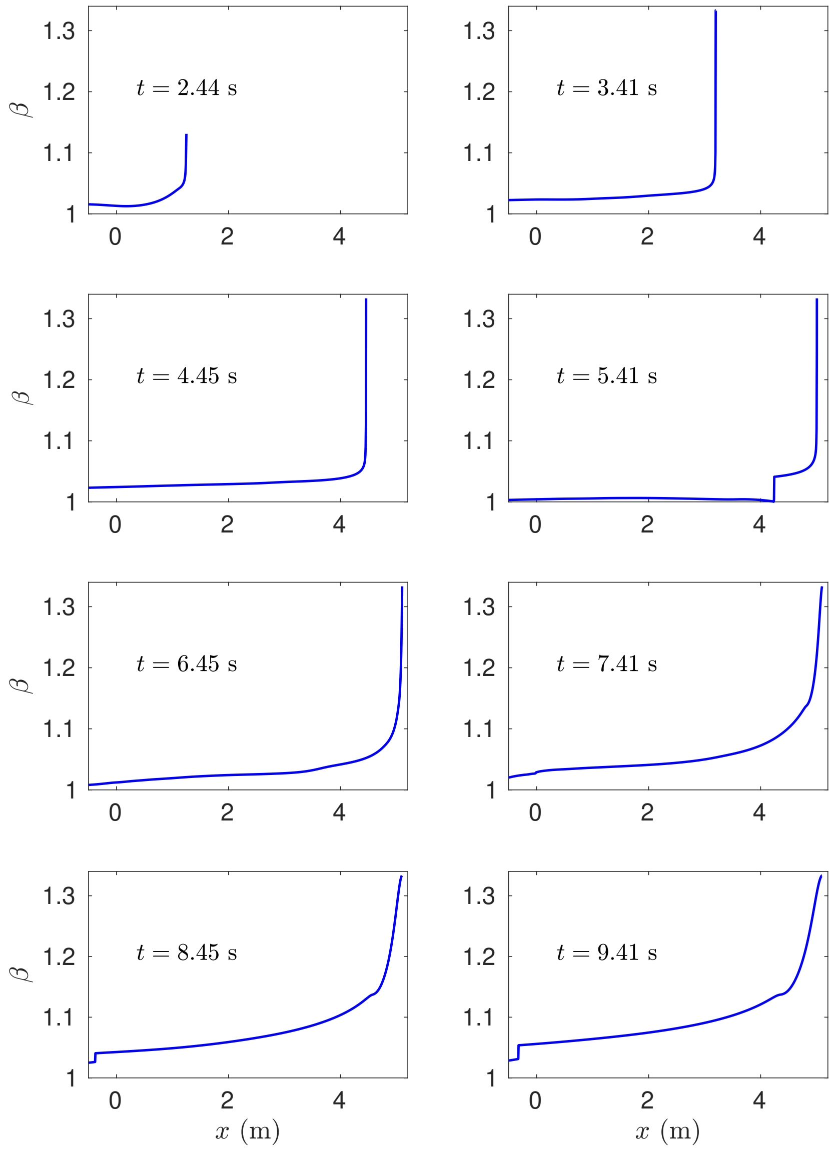

Fig. 4. Snapshots of the modelled flow (β) with $\beta \neq 1$ at different times.

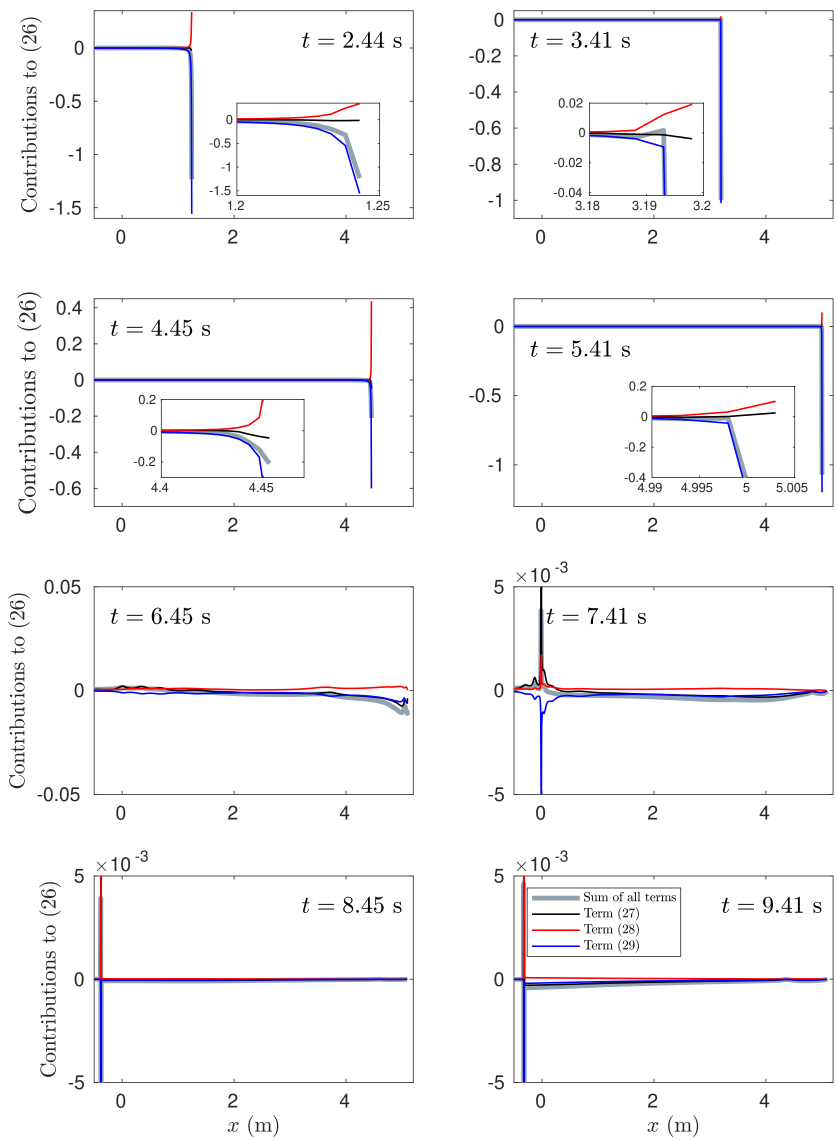

Fig. 5. Snapshots of the terms (27)-(29) during the swash event. All terms are normalised by the maximum magnitude of all non-ϵ (i.e. $\beta = 1$) terms in Eq. (26) at each time for all x.

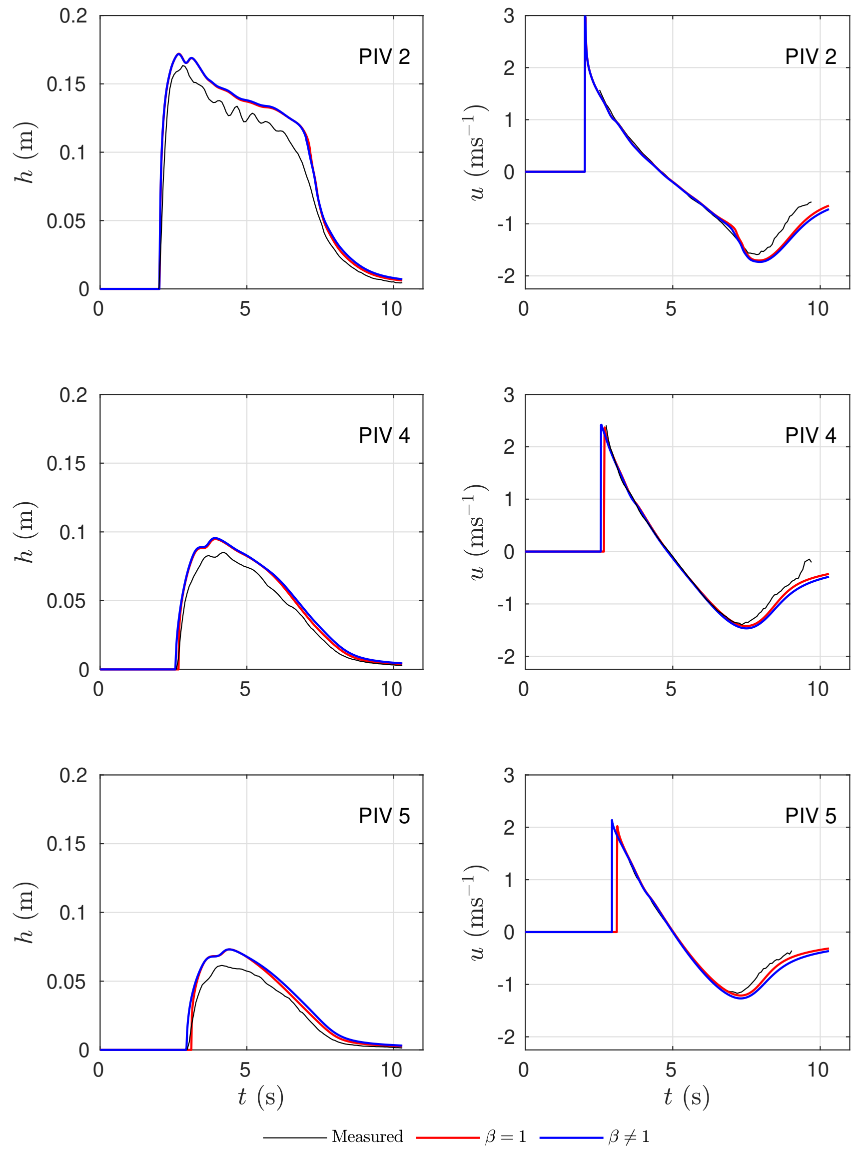

Fig. 6. The comparison of time series of h and u at PIV 2, 4 and 5.

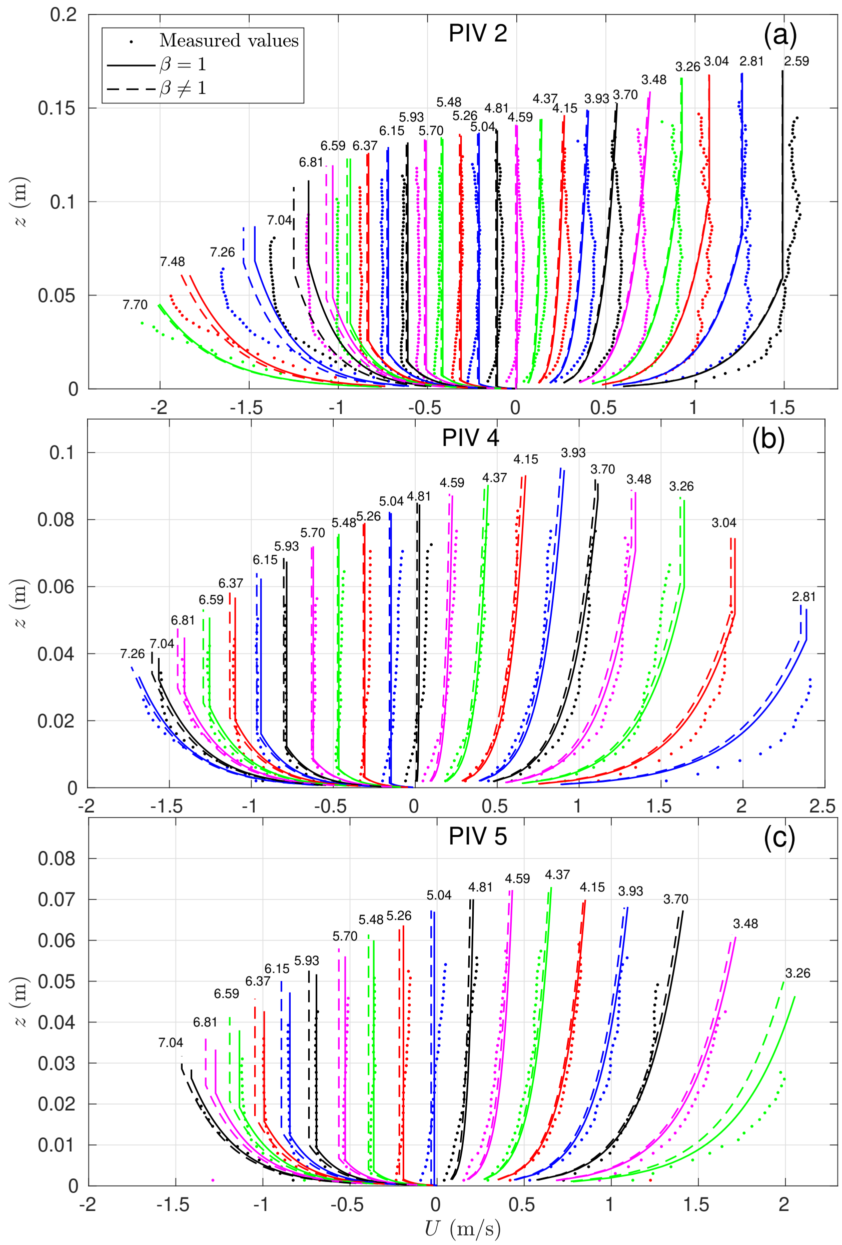

Fig. 7. Comparison between the predicted (solid and dashed coloured lines) and measured (dots) profiles for the horizontal velocity for IMP015 set at PIV 2 (a), 4 (b) and 5 (c); number above each profile is the time. The measured velocities are ensemble-averaged, bed-parallel velocities.

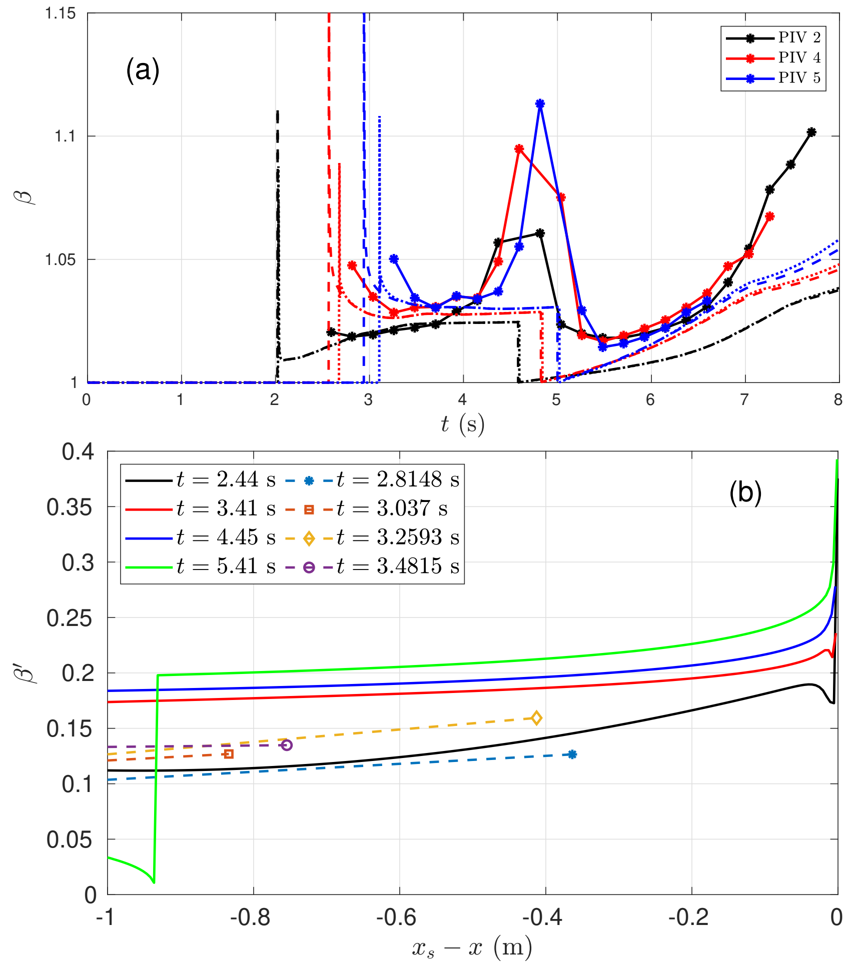

Fig. 8. (a) Comparison between the predicted (dashed ($\beta \neq 1$) and dotted ($\beta = 1$) coloured lines) and measured (solid lines) β values for IMP015 set at PIV 2, 4 and 5. (b) Snapshots of numerical β' (solid lines) at the same times as for Figs. 2–4. Symbols connected by broken lines indicate the calculated values of β' from the measurements at PIV 2, 4 and 5. The horizontal axis is adjusted so as to show the region of uprush 1 m from the swash tip.